CONEM 2022
CONGRESSO NACIONAL DE ENGENHARIA MECÂNICA
TERESINA - PI

ABCM

XI CONGRESSO NACIONAL DE ENGENHARIA MECÂNICA
DE 07 A 11 DE AGOSTO DE 2022, TERESINA-PI, BRASIL

ON THE USE OF GREEN'S THEOREM FOR THE CALCULATION OF GEOMETRIC AND INERTIA PROPERTIES OF PLANE SHAPES

Matheus Basílio Rodrigues Fernandes, matheusmbrf@ita.br[1]
Rubens Gonçalves Salsa Junior, rubens.salsa@ufrn.br[2]
Thiago de Paula Sales, tpsales@ita.br[1]
Domingos Alves Rade, rade@ita.br[1]

[1]Aeronautics Institute of Technology, Pç. Mal. Eduardo Gomes, 50, São José dos Campos, SP 12228-900, Brazil
[2]Federal University of Rio Grande do Norte, Department of Mechanical Engineering, Natal, RN 59078-970, Brazil

Abstract: *Research on undergraduate engineering education has increasingly focused on the systematic integration of engineering disciplines and advanced mathematics, since it is commonly found in related studies that teaching the mathematics curriculum emphasizing its underlying applications is a key factor in promoting a multidisciplinary and conceptual understanding of mathematical concepts. In this context, this work proposes the use of Green's Theorem as a tool capable of exploring the interdisciplinarity between vector calculus and different engineering disciplines, such as statics and dynamics of rigid bodies. More specifically, it is shown how Green's Theorem can be applied to obtain geometric properties (or inertia properties, for materials with constant surface density) of planar shapes, such as area (mass), centroid (center of mass), second moment of area (moment of inertia), and product moment of area (or product of inertia). For polygonal shapes, the predicted values of the geometric/inertia properties are found to coincide with the analytical ones. For shapes with curvilinear boundaries, the obtained expressions generate approximate values, which converge to the analytical results as the contour discretization is refined. The applicability of this methodology is illustrated through the dynamical analysis of a planar mechanism using the Newton-Euler equations. This application also reveals that orbits obtained with respect to an inertial reference frame or with respect to a body-fixed reference frame are the same.*
Keywords: *engineering education, Green's Theorem, planar rigid body dynamics, Newton-Euler equations*

1. INTRODUCTION

Mathematics subjects and concepts form the backbone of various engineering courses, upon which many of their specific disciplines are built. Nevertheless, problems with learning mathematics seem to be a worldwide phenomenon, which in many cases is responsible for students' lack of motivation, problems in subsequent disciplines, and even students dropping out of engineering courses (Alves *et al.*, 2016; Flegg *et al.*, 2012). This has led to a growing interest in the field of mathematics and engineering education regarding the role of mathematics in engineering courses and how it should be taught. As for the perception of its usefulness, Harris *et al.* (2015) discussed that students and lecturers ascribe two distinct values to mathematical knowledge: an use-value, in which mathematical knowledge is seen as a tool for practical use by competent engineers; and an exchange-value, which sees mathematics only as a signal of academic and professional distinction, for which financial reward is expected. They argued that teaching mathematics through abstract and decontextualized examples leads to a loss of perception of its use-value. It was also suggested by them that, whenever possible, mathematics should be taught in an integrated manner with engineering concepts. In the same fashion, Faulkner *et al.* (2019) concluded that teaching through modeling examples and more contextualized problems may help students to learn the fundamental underlying concepts better, as well as improve their motivation. Similar conclusions are also made by Alves *et al.* (2016). With respect to understanding the function of mathematics in the curriculum of engineering courses, Craig (2013) and Harris *et al.* (2015) pointed out that students have a very vague notion of the role that mathematics will play in their future studies and professional career. Wood *et al.* (2012) discussed that this lack of understanding can have significant impacts on students' motivation to learn and can be a barrier to understanding the mathematics they are presented with. On the other hand, as highlighted by Manseur *et al.* (2010), in order to effectively promote interdisciplinary teaching, it is not enough for the teaching of mathematics to be contextualized, but it is also necessary for engineering disciplines to embed mathematics content into their syllabus. As an example, when testing students ability to correctly approach basic problems about elementary mathematics, Willcox and Bounova (2004) reported that while 80% of the students were able to calculate the eigenmodes of a second-order system, only 20% were successful in calculating the mean and standard deviation of a linear function. Interestingly, these students had previously completed an engineering

course which not only revisited the concept of eigenvalues, but also exemplified its application in aerospace systems.

Based on this ubiquitous idea about the importance of contextualized teaching, this paper proposes the use of Green's Theorem as a tool capable of promoting a contextualized teaching of mathematics, and also of embedding and revisiting mathematical subjects, in particular vector calculus, in specific engineering courses. In fact, Willcox and Bounova (2004) found that vector calculus concepts are one of the most problematic for students to grasp in the MIT Department of Aeronautics and Astronautics, despite being widely used in specific engineering disciplines such as fluid mechanics, thermodynamics, and solid mechanics. Specifically, it is shown how Green's Theorem, which is recognized as one of the four fundamental theorems of vector calculus (Marsden, 2011), can be used to obtain meaningful geometric/inertia properties of planar sections. Accurate knowledge of these properties is of main importance, for instance, in structural engineering design (Hibbeler, 2014), dynamic modeling of mechanical systems (Rade, 2018), biomechanics (Crisco and McGovern, 1997), and physically based animations for computer game applications (House and Keyser, 2017). Area, mass, moments and product of inertia and position of the centroid are among the main ones. From these, other important properties can be determined, such as the principal axes and principal moments of inertia. For plantar shapes, these properties are defined and usually computed in terms of double integrals, which can be converted to appropriate line integrals using Green's Theorem. Considering the regions to be composed of connected line segments, a simple analytical expression can be obtained for each of the properties. The main objective of this paper is to develop, verify, analyze and apply those expressions to meaningful engineering problems.

The paper is structured in the following way. After this introduction, the methodology for obtaining the desired geometric/inertia properties using Green's Theorem is addressed. Then, the obtained expressions are validated for four planar shapes of increasingly complexity using analytically computed values. Following, the expressions are applied in obtaining the governing equation of motion for a slider-crank mechanism. Lastly, concluding remarks are presented.

2. GEOMETRIC PROPERTIES OF PLANAR SHAPES USING GREEN'S THEOREM: MATHEMATICAL BACKGROUND

Geometric properties of plane shapes such as area, centroid, moment of inertia, and product of inertia are quantities that can be assessed by computing a double integral over the underlying region. For instance, the area A of a two-dimensional region D can be computed by the following double integral over D:

$$A = \iint_D 1 \, \mathrm{d}A. \tag{1}$$

For relatively simple shapes such as rectangles and circles, the integral expressed in Eq. (1) can be calculated in a relatively simple and straightforward way. However, for complex or non-smooth shapes (cf. Fig. 1), analytical calculation becomes too complicated and error-prone. In these cases, numerical integration methods (Press *et al.*, 2007) such as Gaussian quadratures or Simpson's rules are commonly used. Generally speaking, these techniques evaluate the integrand at a finite set of points, called integration points, and approximate the sought integral through a weighted sum of these values. The integration points and weights vary according to the method considered.

Another alternative, which is proposed in this work, is to calculate the desired integral in an exact fashion, but over a simplified region. As shown in Fig. 1, a general region can be approximated by means of a polygon whose vertices lie on its contour, i.e. by a polygon inscribed in the region. By increasing the number of edges/vertices of the polygon, the simplified region will naturally become more similar to the original shape.

Since the simplified region is now made up of connected straight lines, the integral can be calculated more simply. Alternatively, the double integral over the polygonal region can be recast into a line integral along the line segments that make up its boundary. This can be done using Green's Theorem, which ensures the equivalence between a line integral of a vector field $\mathbf{F}$ and the double integral of the 2D-curl of $\mathbf{F}$. Green's Theorem can be stated as follows (Kreyszig, 2010):

Theorem 1 *Let D be a closed bounded region in the xy plane whose boundary ∂D consists of finitely many smooth curves positively oriented. By positively oriented it is meant that the boundary ∂D is oriented in such a way that D is on the left as ones advances along the curve. Let $F_x(x, y)$ and $F_y(x, y)$ be functions that are continuous and have continuous partial derivatives everywhere on an open region that contains D. Then:*

$$\iint_D \left(\frac{\partial F_y}{\partial x} - \frac{\partial F_x}{\partial y} \right) \mathrm{d}A = \oint_{\partial D} \mathbf{F} \cdot \mathrm{d}\mathbf{r}, \tag{2}$$

where $\mathbf{F}(x, y) = F_x(x, y)\,\mathbf{i} + F_y(x, y)\,\mathbf{j}$, with $\mathbf{i}$ and $\mathbf{j}$ being the unit vectors in the direction of the x and y axes, respectively, of a two-dimensional Cartesian coordinate system.

Therefore, by carefully selecting the vector field $\mathbf{F}$, it is possible to switch from evaluating a double integral over a closed region to computing a line integral along its boundary. For the computation of area, it is chosen the vector field $\mathbf{F}(x, y) = -y\,\mathbf{i} + x\,\mathbf{j}$, since:

$$\iint_D \left(\frac{\partial F_y}{\partial x} - \frac{\partial F_x}{\partial y} \right) \mathrm{d}A = \iint_D 2 \, \mathrm{d}A = 2 \times A. \tag{3}$$

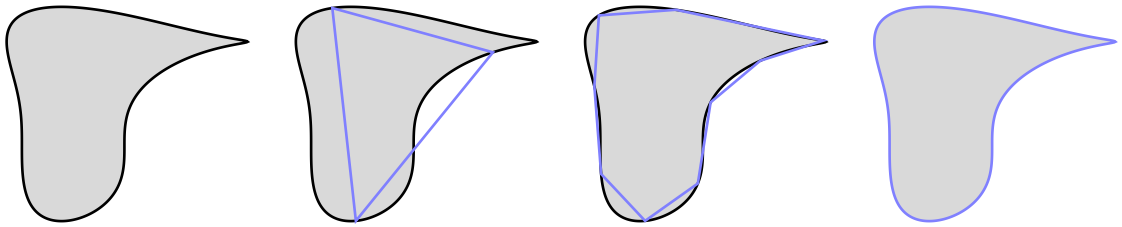

Figure 1: **Approximation of a planar shape as a polygon inscribed to it.**

Here, we assume that the general boundary ∂D can be represented by connected line segments. Thus, we discretize the general boundary by a series of n edges with $n+1$ vertices with coordinates $(x_1, y_1), (x_2, y_2), \ldots, (x_n, y_n), (x_{n+1}, y_{n+1})$. Since the region D is closed, both the first and the last vertices must coincide, i.e., $(x_{n+1}, y_{n+1}) = (x_1, y_1)$.

Let $\mathbf{r}(t)$ be the parametric equation which represents the straight line segment connecting two successive points (x_i, y_i) and (x_{i+1}, y_{i+1}), from the first to the second. It can be written as:

$$\mathbf{r}(t) = [x_i + (x_{i+1} - x_i)t]\,\mathbf{i} + [y_i + (y_{i+1} - y_i)t]\,\mathbf{j}, \qquad 0 \leq t \leq 1. \tag{4}$$

Calculating the line integral in the right-hand side of Eq. (2) along the curve represented by $\mathbf{r}(t)$ yields:

$$\int_{\mathbf{r}} \mathbf{F} \cdot \mathrm{d}\mathbf{r} = \int_{t_0}^{t_1} \mathbf{F}(\mathbf{r}(t)) \cdot \mathbf{r}'(t)\,\mathrm{d}t \tag{5}$$

$$= \int_0^1 \{-[y_i + (y_{i+1} - y_i)t]\,\mathbf{i} + [x_i + (x_{i+1} - x_i)t]\,\mathbf{j}\} \cdot \{(x_{i+1} - x_i)\,\mathbf{i} + (y_{i+1} - y_i)\,\mathbf{j}\}\,\mathrm{d}t \tag{6}$$

$$= \int_0^1 (x_i y_{i+1} - x_{i+1} y_i)\,\mathrm{d}t = x_i y_{i+1} - x_{i+1} y_i. \tag{7}$$

Applying Green's Theorem on the successive line segments which constitute the discretized boundary ∂D yields:

$$A = \frac{1}{2}\iint_D 2\,\mathrm{d}A = \frac{1}{2}\oint_{\partial D} \mathbf{F} \cdot \mathrm{d}\mathbf{r} = \frac{1}{2}\oint_{\mathbf{r}_1 + \mathbf{r}_2 + \ldots + \mathbf{r}_n} \mathbf{F} \cdot \mathrm{d}\mathbf{r} \tag{8}$$

$$= \frac{1}{2}\left(\int_{\mathbf{r}_1} \mathbf{F} \cdot \mathrm{d}\mathbf{r} + \int_{\mathbf{r}_2} \mathbf{F} \cdot \mathrm{d}\mathbf{r} + \cdots + \int_{\mathbf{r}_n} \mathbf{F} \cdot \mathrm{d}\mathbf{r}\right) \tag{9}$$

$$= \frac{1}{2}\left[(x_1 y_2 - x_2 y_1) + (x_2 y_3 - x_3 y_2) + \cdots + (x_n y_{n+1} - x_{n+1} y_n)\right] \tag{10}$$

$$= \frac{1}{2}\sum_{i=1}^{n} (x_i y_{i+1} - x_{i+1} y_i). \tag{11}$$

The expression given in Eq. (11) allows approximating the area of the original region by means of an algebraic expression that depends only on the coordinates of the vertices of the surrogate region. Furthermore, since it is written as a sum, it can be implemented computationally in a very straightforward and simple way.

The vector field chosen is just one of a multitude of other possible fields. In fact, it is possible to choose any other vector field as long as $(\partial F_y/\partial x - \partial F_x/\partial y)$ is a constant and the continuity requirements of Green's Theorem for the components of $\mathbf{F}$ and their partial derivatives are satisfied. Although the expression that would be obtained after computing the integral using another vector field may differ, the summation along the edges of the polygon must produce the same result. To illustrate this, consider the vector field $\mathbf{F}(x, y) = -y\,\mathbf{i}$, which is also suitable for computing the area of the region. In this case the double integral produces directly the area, since:

$$\iint_D \left(\frac{\partial F_y}{\partial x} - \frac{\partial F_x}{\partial y}\right)\mathrm{d}A = \iint_D 1\,\mathrm{d}A. \tag{12}$$

Calculating the line integral in the right-hand side of Eq. (2) along the curve $\mathbf{r}(t)$ for the alternative vector field $\mathbf{F}$

yields:

$$\int_r \mathbf{F}\cdot\mathrm{d}\mathbf{r} = \int_{t_0}^{t_1} \mathbf{F}(\mathbf{r}(t))\cdot\mathbf{r}'(t)\,\mathrm{d}t \tag{13}$$

$$= \int_0^1 \{-[y_i+(y_{i+1}-y_i)t]\,\mathbf{i}\cdot\{(x_{i+1}-x_i)\,\mathbf{i}+(y_{i+1}-y_i)\,\mathbf{j}\}\,\mathrm{d}t = \frac{1}{2}(x_i-x_{i+1})(y_i+y_{i+1}), \tag{14}$$

such that the area can be computed as:

$$A = \frac{1}{2}\sum_{i=1}^{n}(x_i-x_{i+1})(y_i+y_{i+1}). \tag{15}$$

This equation can be further manipulated to produce:

$$A = \frac{1}{2}\sum_{i=1}^{n}(x_iy_i - x_{i+1}y_{i+1} + x_iy_{i+1} - x_{i+1}y_i) = \frac{1}{2}\sum_{i=1}^{n}(x_iy_i - x_{i+1}y_{i+1}) + \frac{1}{2}\sum_{i=1}^{n}(x_iy_{i+1} - x_{i+1}y_i). \tag{16}$$

It is easy to see that the first summation results in zero. Expanding this summation ones gets:

$$\frac{1}{2}\sum_{i=1}^{n}(x_iy_i - x_{i+1}y_{i+1}) = \frac{1}{2}\left[(x_1y_1 - x_2y_2) + (x_2y_2 - x_3y_3) + \cdots + (x_ny_n - x_{n+1}y_{n+1})\right] = 0, \tag{17}$$

since, as previously stated, $(x_1, y_1) = (x_{n+1}, y_{n+1})$. Therefore, the resulting expression of Eq. (16) coincides with the expression obtained in Eq. (11). It is emphasized that, although the choice of vector field is somewhat arbitrary, the curve must be parameterized in the positive orientation. The incorrect parametrization will give an incorrect sign generating, for instance, a negative area.

The same procedure can be applied for calculating another geometric properties of planar shapes, such as the x- and y-components of the centroid ($\bar{x}$ and $\bar{y}$), the area moments of inertia about the x- and y-axis (I_{xx} and I_{yy}) and the area product of inertia about the x- and y-axis (I_{xy}). These properties are defined by the following double integrals (Hibbeler, 2014):

$$\bar{x} = \frac{1}{A}\iint_D x\,\mathrm{d}A, \quad \bar{y} = \frac{1}{A}\iint_D y\,\mathrm{d}A, \quad I_{xx} = \iint_D y^2\,\mathrm{d}A, \quad I_{yy} = \iint_D x^2\,\mathrm{d}A, \quad I_{xy} = \iint_D xy\,\mathrm{d}A. \tag{18}$$

For each of these properties, the chosen vector fields and the resulting algebraic expressions are given in Tab. 1. The integrands of the line integrals resulting from applying Green's Theorem are all polynomials in t and, therefore, easy to compute. Accordingly, the details concerning their calculation are omitted.

Table 1: **Vector fields and resulting algebraic expressions for several geometric properties.**

Property	**Chosen $\mathbf{F}(x,y)$**	**Resulting expression**
Area	$-y\,\mathbf{i} + x\,\mathbf{j}$	$A = \frac{1}{2}\sum_{i=1}^{n}(x_iy_{i+1} - x_{i+1}y_i)$
x-component of the centroid	$-xy\,\mathbf{i} + x^2\,\mathbf{j}$	$\bar{x} = \frac{1}{6A}\sum_{i=1}^{n}(x_i + x_{i+i})(x_iy_{i+1} - x_{i+1}y_i)$
y-component of the centroid	$-y^2\,\mathbf{i} + xy\,\mathbf{j}$	$\bar{y} = \frac{1}{6A}\sum_{i=1}^{n}(y_i + y_{i+i})(x_iy_{i+1} - x_{i+1}y_i)$
Area moment of inertia about the x-axis	$-y^3\,\mathbf{i} + xy^2\,\mathbf{j}$	$I_{xx} = \frac{1}{12}\sum_{i=1}^{n}(y_i^2 + y_iy_{i+1} + y_{i+1}^2)(x_iy_{i+1} - x_{i+1}y_i)$
Area moment of inertia about the y-axis	$-x^2y\,\mathbf{i} + x^3\,\mathbf{j}$	$I_{yy} = \frac{1}{12}\sum_{i=1}^{n}(x_i^2 + x_ix_{i+1} + x_{i+1}^2)(x_iy_{i+1} - x_{i+1}y_i)$
Area product of inertia about the x- and y-axis	$-xy^2\,\mathbf{i} + x^2y\,\mathbf{j}$	$I_{xy} = \frac{1}{24}\sum_{i=1}^{n}[(x_iy_{i+1} + 2(x_iy_i + x_{i+1}y_{i+1}) + x_{i+1}y_i)(x_iy_{i+1} - x_{i+1}y_i)]$

It is worth to point out that all algebraic equations given in Tab. 1 produce the exact value for their respective property when D is a polygonal shape. This stems from the fact that no approximation is involved in the calculation of the integral given by Eq. (2). The only approximation made in the methodology was the substitution of the original boundary by a series of connected line segments. Therefore, if the original contour is already composed of line segments, the integral calculation must be exact. Otherwise, for the case when the boundary ∂D is constituted by curved lines, the obtained result will be just approximated, converging to the exact value as the number of considered line segments approaches infinity (cf. Fig. 1).

3. RESULTS AND DISCUSSION

This section aims to validate and show the application of the expressions given in Tab. 1 for the computation of geometric/inertia properties of planar shapes. First, the values predicted by these expressions are compared to the analytical ones for four plane sections of increasing complexity. Next, it is shown how the expressions obtained for the moments of inertia I_{xx} ans I_{yy} can be applied to verify the equivalence of Newton-Euler equations, whether written in an inertial or non-inertial (body-fixed) frame of reference.

3.1 Validation and Convergence Study

In order to validate and verify the accuracy of the obtained expressions (cf. Tab. 1), this subsection considers the geometric properties of the four plane shapes shown in Fig. 2. They concern, respectively, an I-shaped section, a circular section, a square section with a circular hole, and a complex shape formed by three semicircles, with ellipsoidal and rhombus-shaped holes. For the sake of simplicity, hereinafter these forms will be referred to as sections I, II, III, and IV, respectively. The relevant dimensions of the sections can be readily read from the axes of the plots.

For each section, Tab. 2 shows the analytical and approximate values obtained for each of the properties of interest. The error of the approximated value, here defined as the percentage deviation from the analytical value, is also reported. The discretization level of the curved boundaries was taken as the minimum necessary to produce a maximum error of 0.1%.

The results shown in Tab. 2 verify the validity of the obtained expressions. They also show some interesting features. First, it is noted that the values computed for the section I are exact. As discussed earlier, the only approximation involved in the methodology concerns the discretization of the boundary of the plane shape. As the I-shaped section already presents a polygonal shape, there is no approximation involved at all, so that the results obtained are exact. Second, the extremely small errors found for the centroid position of sections II and III are remarkable. This is due to the fact that even a coarse discretization can create a shape which preserves the general arrangement of the actual region, leading to results close to the analytical ones for the centroid position. In fact, the section size-dependent properties (area, and moments and product of inertia) in general showed greater errors compared to those for the centroid position, which is by definition area-normalized. Third, it can be seen that less edges were required for the section II as compared to the section III to reach the desired accuracy, even though the circles existing in both shapes have the same radius. Since the expressions in Tab. 1 produce exact values for straight lines, the overall accuracy is influenced only by any existing curved boundaries. For such regions, the larger the perimeter of the curved contours (relative to the total perimeter), the more edges are required to achieve a given accuracy. Likewise, for section IV, whose contours are formed mainly by non-straight lines, the amount of edges required to achieve the same percentage error was significantly larger. In this sense, when more than one curvilinear contour exists, it becomes interesting to discretize them with the number of edges for each curve being proportional to its length. This was the discretization strategy adopted for section IV.

The discussions provided above are ratified by Figs. 3 and 4. Figure 3 shows a convergence study for the properties of section III as the number of edges discretizing its inner circle is increased. Due to the symmetry of the shape, the errors are equal for both I_{xx} and I_{yy}, as well as for A and I_{xy}. Figure 3(a) shows that all estimated values showed a decreasing error with increasing number of edges. As shown in Fig. 3(b), even very coarse discretizations (whose number of vertices is close to zero) produce an error around the machine precision for the position of the centroid. As discussed earlier, this

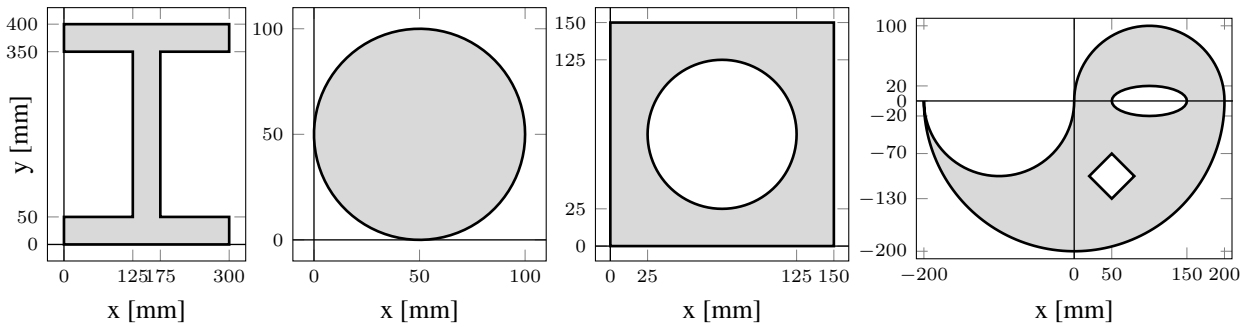

(a) Section I (b) Section II (c) Section III (d) Section IV

Figure 2: **Planar shapes under analysis.**

Table 2: **Comparison between approximate and analytical values for geometric properties of the four planar shapes under study.**

	Value	Section I	Section II	Section III	Section IV
Number of edges	-	12	89	64	141
Area [mm^2]	Exact	4.5×10^4	7.8540×10^3	1.4646×10^4	5.7890×10^4
	Approximated	4.5×10^4	7.8474×10^3	1.4660×10^4	5.7866×10^4
	Error	0%	0.0830%	0.0980%	0.041%
$\bar{x}$ [mm]	Exact	150	50	75	47.2866
	Approximated	150	50	75.0000	47.2906
	Error	0%	8.526×10^{-14}%	0%	0.008%
$\bar{y}$ [mm]	Exact	200	50	75	-65.9869
	Approximated	200	50	75.0000	-65.9650
	Error	0%	8.526×10^{-14}%	1.8948×10^{-14}%	0.033%
I_{xx} [mm^4]	Exact	2.8375×10^9	2.4544×10^7	1.1966×10^8	6.0973×10^8
	Approximated	2.8375×10^9	2.4519×10^7	1.1976×10^8	6.0914×10^8
	Error	0%	0.0996%	0.0824%	0.097%
I_{yy} [mm^4]	Exact	1.240625×10^9	2.4544×10^7	1.1966×10^8	5.9017×10^8
	Approximated	1.240625×10^9	2.4519×10^7	1.1976×10^8	5.8964×10^8
	Error	0%	0.0996%	0.0824%	0.089%
I_{xy} [mm^4]	Exact	1.35×10^9	1.9635×10^7	8.2384×10^7	9×10^6
	Approximated	1.35×10^9	1.9619×10^7	8.2465×10^7	9.0000×10^6
	Error	0%	0.0830%	0.0980%	1.45×10^{-13}%

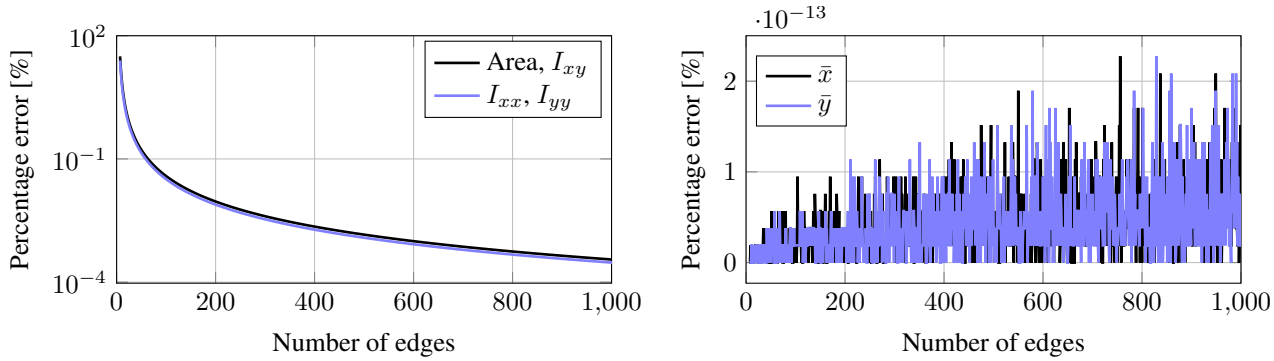

(a) (b)

Figure 3: **Convergence for the properties of section III as the number of edges discretizing its inner circle is increased.**

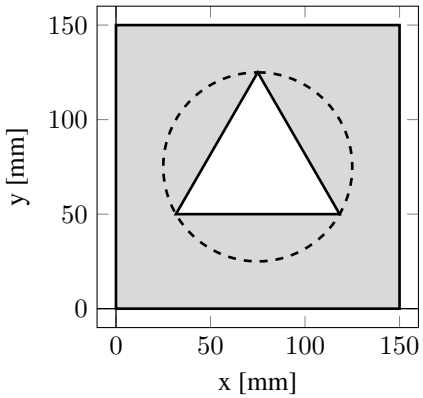

Figure 4: **Discretization of the inner circle of section III using only 3 vertices.**

is due to the symmetry of the surrogate section for every discretization level. Even when the inner circle is discretized with only 3 edges (cf. Fig. 4), the symmetry of the plane shape is kept, causing the error for the centroid position to be virtually zero.

3.2 Application in Rigid Body Dynamics

The previous section showed the direct application of the expressions in Tab. 1 in computing the geometric properties of planar shapes. This section aims to illustrate how they can be applied in the study of planar dynamics of rigid bodies. Under the Newton-Euler formalism, the equations of motion for a rigid body can be obtained by applying the following equations, which establish the balance of linear and angular momenta:

$$\mathbf{F}^{\text{tot}} = \dot{\mathbf{L}}, \qquad \text{where} \quad \mathbf{L} = m \cdot \mathbf{v}_{\text{CM}}, \tag{19}$$

$$\mathbf{M}_{\text{P}}^{\text{tot}} = \dot{\mathbf{H}}_{\text{P}}, \qquad \text{where} \quad \mathbf{H}_{\text{P}} = \mathbf{J}_{\text{P}} \cdot \boldsymbol{\omega} + m \cdot \mathbf{r}_{\text{CM/P}} \times \mathbf{v}_{\text{P}}, \tag{20}$$

where m is the mass of the body, $\mathbf{v}_{\text{CM}}$ is the velocity of its center of mass, $\mathbf{J}_P$ is the inertia tensor of the body about point P (which is assumed attached to the body), $\boldsymbol{\omega}$ is the angular velocity of the body, $\mathbf{r}_{\text{CM/P}}$ is a vector denoting the position of its center of mass relative to point P, and $\mathbf{v}_{\text{P}}$ is the velocity of point P; $\mathbf{F}^{\text{tot}}$ is the resultant force and $\mathbf{M}_{\text{P}}^{\text{tot}}$ is the resultant moment (about P) applied to the rigid body.

The inertia tensor is formed by the mass moments and products of inertia. These can be obtained from the area moments and products of inertia, whose expressions are given in Tab. 1. For a rigid body of uniform density ρ and constant thickness t, they are related by:

$$J_{ij} = \iiint_V ij \ \mathrm{d}m = \iiint_V ij \times \rho \ \mathrm{d}V = \iint_D ij \times \rho t \ \mathrm{d}A \tag{21}$$

$$= \sigma \iint_D ij \ \mathrm{d}A = \sigma \times I_{ij}, \quad \text{with } i \text{ and } j = x, y, z, \tag{22}$$

with σ being the area density of the rigid body.

The vectors and the tensor present in Eqs. (19) and (20) can be represented in any frame of reference. It is common practice to write the angular momentum vector in a body-fixed reference frame (hereinafter referred to as body frame), denoted as $\mathscr{B}$, because its components are time-independent in this representation, making it simpler to compute the time derivative of the angular momentum vector. Under this assumption, the Euler's equation given in Eq. (20) can be expanded as (Santos, 2001):

$${}_{\mathscr{B}}\mathbf{M}_{\text{P}}^{\text{tot}} = {}_{\mathscr{B}}\mathbf{J}_{\text{P}} \cdot {}_{\mathscr{B}}\dot{\boldsymbol{\omega}} + {}_{\mathscr{B}}\boldsymbol{\omega} \times \left({}_{\mathscr{B}}\mathbf{J}_{\text{P}} \cdot {}_{\mathscr{B}}\boldsymbol{\omega} \right) + m \cdot {}_{\mathscr{B}}\mathbf{r}_{\text{CM/P}} \times {}_{\mathscr{B}}\mathbf{a}_{\text{P}}, \tag{23}$$

where ${}_{\mathscr{B}}\mathbf{a}_{\text{P}}$ is the acceleration of point P. The left subscript denotes the frame of reference in which the vector or tensor is represented. It can be seen from Eq. (23) that this approach indeed circumvents the need to differentiate the components of the inertia tensor with respect to time. Alternatively, the vectors and tensor in Eqs. (19) and (20) can be written with respect to an inertial reference frame $\mathscr{I}$. In this case, Eq. (20) can be expressed as:

$${}_{\mathscr{I}}\mathbf{M}_{\text{P}}^{\text{tot}} = \frac{\mathrm{d}}{\mathrm{d}t} \left({}_{\mathscr{I}}\mathbf{J}_{\text{P}} \cdot {}_{\mathscr{I}}\boldsymbol{\omega} + m \cdot {}_{\mathscr{I}}\mathbf{r}_{\text{CM/P}} \times {}_{\mathscr{I}}\mathbf{v}_{\text{P}} \right) \tag{24}$$

$$= {}_{\mathscr{I}}\dot{\mathbf{J}}_{\text{P}} \cdot {}_{\mathscr{I}}\boldsymbol{\omega} + {}_{\mathscr{I}}\mathbf{J}_{\text{P}} \cdot {}_{\mathscr{I}}\dot{\boldsymbol{\omega}} + \frac{\mathrm{d}}{\mathrm{d}t} \left(m \cdot {}_{\mathscr{I}}\mathbf{r}_{\text{CM/P}} \times {}_{\mathscr{I}}\mathbf{v}_{\text{P}} \right), \tag{25}$$

for which the time dependence of the components of the inertia tensor are explicitly represented.

Although Euler's equation is guaranteed to yield the same set of differential equations whether written with respect to a body frame or to an inertial one, Eq. (23) is used almost exclusively to obtain the equations of motion of mechanical systems, since the components of the inertia tensor are constant in the body frame (Rade, 2018). To verify this equivalence, the equation of motion governing the dynamics of the slider-crank mechanism shown in Fig. 5 is derived using Euler's equation written in both the inertial and the body frames. This mechanism is widely used to convert straight-line reciprocating motion to rotary motion or vice versa (Ha *et al.*, 2006). While the slider and the crank develop purely translational and rotational motions, respectively, the connecting rod undergoes general planar motion. For simplicity, the mass of the slider is neglected in the analysis that follows. The system is driven by a moment $M(t)$ applied to the crank, and possesses only one degree of freedom, which is taken to be the angle $\theta(t)$ made by the crank with the horizontal. In addition to the inertial, two auxiliary reference frames are employed. The first, denoted as $\mathscr{B}_1$, has point O as its origin and rotates attached to the crank. The reference frame $\mathscr{B}_2$, in turn, has its origin at point B and is rigidly attached to the connecting rod.

Since the motion of the mechanism is restricted to the xy plane, the only moment of inertia required to obtain the equation of motion is J_{zz}. As the crank describes a rotation around a fixed axis, its moment of inertia J_{zz} is the same with respect to both the inertial and the body frames. Appendix A shows how the expressions shown in Tab. 1 can be used to reach this conclusion. On the other hand, the connecting rod presents a moment of inertia J_{zz} which, when described in the inertial frame, varies with time. To compute it, first the position vectors of its vertices are written in terms of its body frame, as follows:

$${}_{\mathscr{B}_2}\mathbf{r}_{\text{P}_1/\text{B}} = [0 \quad h/2 \quad 0]^\top, \quad {}_{\mathscr{B}_2}\mathbf{r}_{\text{P}_2/\text{B}} = [-L \quad h/2 \quad 0]^\top, \quad {}_{\mathscr{B}_2}\mathbf{r}_{\text{P}_3/\text{B}} = [-L \quad -h/2 \quad 0]^\top, \quad {}_{\mathscr{B}_2}\mathbf{r}_{\text{P}_4/\text{B}} = [0 \quad -h/2 \quad 0]^\top, \tag{26}$$

where the vertices $\mathrm{P}_1, \ldots, \mathrm{P}_4$ are defined from point B (cf. Fig. 5), traversing the boundary of the connecting rod in a counterclockwise direction.

These vectors can be written with respect to the inertial reference frame using the transformation matrix $\mathbf{T}_\beta$ and the position vector of point B relative to point O:

$$ {}_{\mathscr{I}}\mathbf{r}_{\mathrm{P_j/B}} = {}_{\mathscr{I}}\mathbf{r}_{\mathrm{B/O}} + {}_{\mathscr{I}}\mathbf{r}_{\mathrm{P_j/B}} = {}_{\mathscr{I}}\mathbf{r}_{\mathrm{B/O}} + \mathbf{T}_\beta^\top \cdot {}_{\mathscr{B}_2}\mathbf{r}_{\mathrm{P_j/B}}, \quad j = 1, \ldots, 4, \tag{27} $$

where:

$$ \mathbf{T}_\beta = \begin{bmatrix} \cos\beta & -\sin\beta & 0 \\ \sin\beta & \cos\beta & 0 \\ 0 & 0 & 1 \end{bmatrix}. \tag{28} $$

Substituting the components of $\mathbf{r}_{\mathrm{P_j/B}}$ into the expressions given in Tab. 1, the following expressions for the moments of inertia $J^{(2)}_{xx,\mathrm{O}}$ and $J^{(2)}_{yy,\mathrm{O}}$ can be found:

$$ J^{(2)}_{xx,\mathrm{O}} = m^{(2)} \left(\frac{L^2 \sin^2\beta}{3} - Lr \sin\beta \sin\theta + \frac{h^2 \cos^2\beta}{12} + r^2 \sin^2\theta \right), \tag{29} $$

$$ J^{(2)}_{yy,\mathrm{O}} = m^{(2)} \left(\frac{L^2 \cos^2\beta}{3} + Lr \cos\beta \cos\theta + \frac{h^2 \sin^2\beta}{12} + r^2 \cos^2\theta \right). \tag{30} $$

The superscript to the right of a quantity denotes the body to which it refers. From Eqs. (29) and (30) the moment of inertia $J^{(2)}_{zz,\mathrm{O}}$ can be readily obtained:

$$ J^{(2)}_{zz,\mathrm{O}} = J^{(2)}_{xx,\mathrm{O}} + J^{(2)}_{yy,\mathrm{O}} = m^{(2)} \left(\frac{L^2}{3} + \frac{h^2}{12} + r^2 + Lr \cos(\beta + \theta) \right), \tag{31} $$

which shows that $J^{(2)}_{zz,\mathrm{O}}$ depends on β and θ and therefore on time.

Figure 6 shows free-body diagrams for the bodies that compose the mechanism. Based on them, the application of Euler's equation to the connecting rod, represented in the inertial frame, is given by:

$$ {}_{\mathscr{I}}\mathbf{r}_{\mathrm{CM_2/O}} \times {}_{\mathscr{I}}\mathbf{F}_{\mathrm{CM_2}} + {}_{\mathscr{I}}\mathbf{r}_{\mathrm{A/O}} \times \left(-{}_{\mathscr{I}}\mathbf{F}_{\mathrm{A}}\right) + {}_{\mathscr{I}}\mathbf{r}_{\mathrm{B/O}} \times {}_{\mathscr{I}}\mathbf{F}_{\mathrm{B}} = {}_{\mathscr{I}}\dot{\mathbf{J}}_{\mathrm{O}} \cdot {}_{\mathscr{I}}\boldsymbol{\omega}^{(2)} + {}_{\mathscr{I}}\mathbf{J}_{\mathrm{O}} \cdot {}_{\mathscr{I}}\dot{\boldsymbol{\omega}}^{(2)} + \frac{\mathrm{d}}{\mathrm{d}t}\left(m \cdot {}_{\mathscr{I}}\mathbf{r}_{\mathrm{CM/O}} \times {}_{\mathscr{I}}\mathbf{v}_{\mathrm{O}} \right). \tag{32} $$

Expanding and simplifying Eq. (32), one gets:

$$ -m^{(2)} g \left(r\cos\theta + \frac{L}{2}\cos\beta \right) - F_{\mathrm{A}y} r\cos\theta + F_{\mathrm{A}x} r\sin\theta + F_{\mathrm{B}y}(r\cos\theta + L\cos\beta) = -\dot{I}^{(2)}_{zz,\mathrm{O}}\dot{\beta} - J^{(2)}_{zz,\mathrm{O}}\ddot{\beta} \tag{33} $$

$$ + m^{(2)} r^2 \left(\ddot{\beta} + \ddot{\theta} \right) + m^{(2)} r \frac{L}{2} \left[\cos(\beta + \theta) \left(\ddot{\beta} + \ddot{\theta} \right) - \sin(\beta + \theta) \left(\dot{\beta} + \dot{\theta} \right)^2 \right], \tag{34} $$

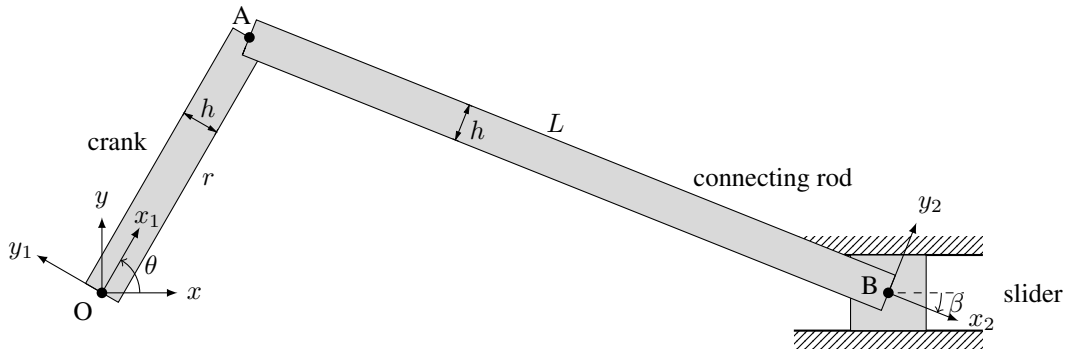

Figure 5: **Slider-crank mechanism under study.**

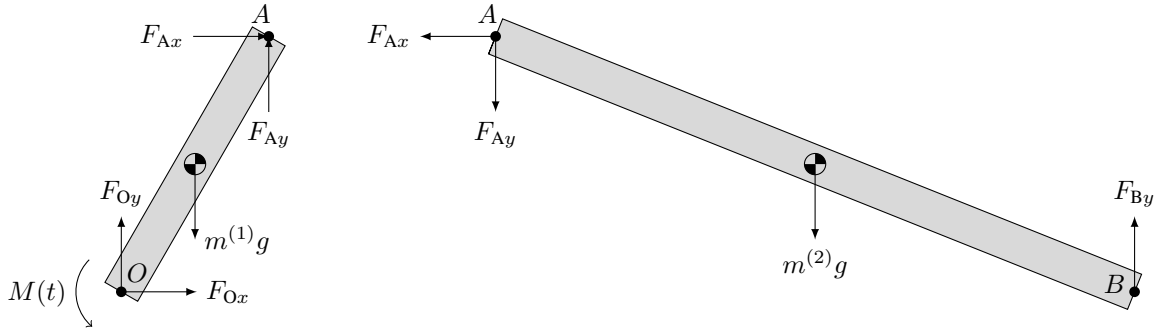

Figure 6: **Free-body diagram for the slider-crank mechanism under study.**

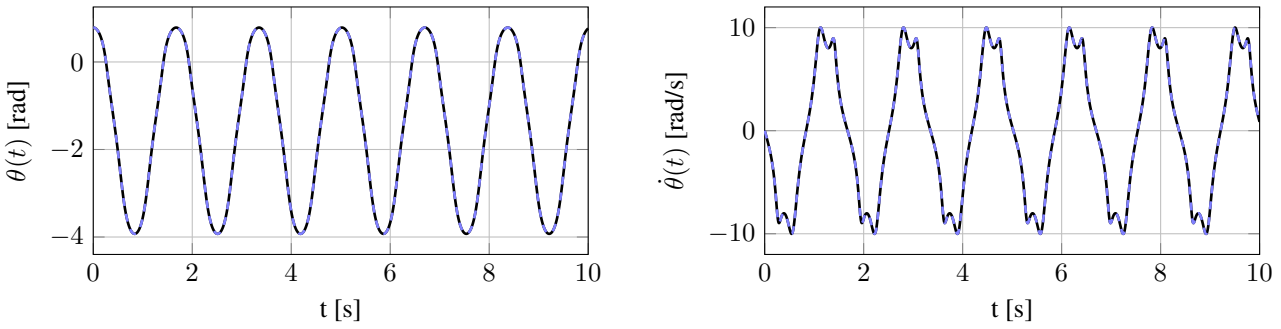

Figure 7: **$\theta(t)$ and $\dot{\theta}(t)$ for the slider-crank mechanism due to initial conditions $\theta_0 = \pi/4$ rad and $\dot{\theta}_0 = 0$ rad/s. ——: results obtained using Eq. (34); - - - : results obtained using Eq. (37).**

where the time derivative of the moment of inertia $J^{(2)}_{zz,\mathrm{O}}$ can be computed using Eq. (31), being given by:

$$\dot{J}^{(2)}_{zz,\mathrm{O}} = -m^{(2)} L r \sin(\beta+\theta)(\dot{\beta}+\dot{\theta}). \tag{35}$$

Newton's equations for the crank and connecting rod, along with Euler's equation for the crank (all provided in Appendix B) and Eq. (33) can be combined to obtain the equation of motion for the slider-crank mechanism, which is given by:

$$\begin{aligned}
&4\left[m^{(2)}L^3 r\cos^2\beta\sin\theta\sin\beta - m^{(2)}Lr^3\cos\beta\cos\theta\cos(2\theta) - m^{(2)}r^4\cos^4\theta + J^{(1)}_{zz,\mathrm{O}}L^2\cos^2\beta + J^{(2)}_{zz,\mathrm{O}}r^2\cos^2\theta\right]\ddot{\theta}\\
&= 4L^2M(t)\cos^2\beta + 2r^2\sin(2\theta)J^{(2)}_{zz,\mathrm{O}}\left(\dot{\theta}^2-\dot{\beta}^2\right) - 2L^2 g(m^{(1)}+m^{(2)})r\cos^2\beta\cos\theta - 4r^2\cos^2\theta\dot{\theta}\dot{I}^{(2)}_{zz,\mathrm{O}}\\
&+ m^{(2)}L^2r^2\sin(2\beta)\dot{\theta}^2 + 2m^{(2)}r^4\sin(2\theta)\dot{\beta}^2 - 2m^{(2)}L^2r^2\sin(2\theta)\dot{\beta}^2\left(1+\cos^2\beta\right)\\
&\qquad - m^{(2)}L^4\sin(2\beta)\dot{\beta}^2\left(1+2\cos^2\beta\right) - 4m^{(2)}L^3 r\dot{\beta}\cos^2\beta\sin(\beta+\theta)\left(\dot{\beta}+\dot{\theta}\right)
\end{aligned} \tag{36}$$

For a given set of initial conditions $\theta(t=0)=\theta_0$, $\dot{\theta}(t=0)=\dot{\theta}_0$, this equation can be integrated numerically to obtain $\theta(t)$, $\dot{\theta}(t)$. Euler's equation for the connecting rod can also be written with respect to the frame $\mathscr{B}_2$, which is attached to it at point B. Applying Eq. (23) one gets:

$${}_{\mathscr{B}_2}\mathbf{r}_{\mathrm{CM_2/B}} \times_{\mathscr{B}_2} \mathbf{F}_{\mathrm{CM_2}} +_{\mathscr{B}_2}\mathbf{r}_{\mathrm{A/B}} \times \left(-_{\mathscr{B}_2}\mathbf{F}_{\mathrm{A}}\right) =_{\mathscr{B}_2}\mathbf{J}^{(2)}_{\mathrm{B}} \cdot_{\mathscr{B}_2}\dot{\boldsymbol{\omega}}^{(2)} +_{\mathscr{B}_2}\boldsymbol{\omega}^{(2)} \times \left(_{\mathscr{B}_2}\mathbf{J}^{(2)}_{\mathrm{B}} \cdot_{\mathscr{B}_2}\boldsymbol{\omega}^{(2)}\right) + m^{(2)} \cdot_{\mathscr{B}_2}\mathbf{r}_{\mathrm{CM/B}} \times_{\mathscr{B}_2}\mathbf{a}_{\mathrm{B}}, \tag{37}$$

which can be simplified to:

$$(F_{\mathrm{A}y}\cos\beta + F_{\mathrm{A}x}\sin\beta)L + m^{(2)}g\frac{L}{2}\cos\beta = -J^{(2)}_{zz,\mathrm{B}}\ddot{\beta} + m^{(2)}\frac{L}{2}(L\ddot{\beta} + r\dot{\theta}^2\sin(\beta+\theta) - r\ddot{\theta}\cos(\beta+\theta)). \tag{38}$$

It is emphasized that the moment of inertia $J^{(2)}_{zz,\mathrm{B}}$ is calculated with respect to the body frame. It can be easily computed using the expressions given in Tab. 1 and the position vectors given in Eq. (26). The resulting equation of motion for the mechanism can be found by combining Eq. (38) with the Newton's equations for the crank and connecting rod, along with Euler's equation for the crank. This time, it can be written as:

$$\begin{aligned}
&2\left[m^{(2)}L^2r^2\cos\beta\sin\theta\sin(\beta+\theta) + J^{(1)}_{zz,\mathrm{O}}L^2\cos^2\beta + J^{(2)}_{zz,\mathrm{B}}r^2\cos^2\theta\right]\ddot{\theta}\\
&= 2L^2M(t)\cos^2\beta - (m^{(1)}+m^{(2)})grL^2\cos\theta\cos^2\beta - m^{(2)}rL^2\cos\beta(L\dot{\beta}^2\sin\theta - r\dot{\theta}^2\sin(2\theta+\beta))\\
&\qquad + J^{(2)}_{zz,\mathrm{B}}r^2\sin(2\theta)(\dot{\theta}^2-\dot{\beta}^2).
\end{aligned} \tag{39}$$

Both Eqs. (36) and (39) represent the equation of motion for the slider-crank mechanism under consideration. Although it is laborious to show analytically that they can be reduced to the same expression, it is easy to verify that they yield the same values for $\theta(t)$ and $\dot{\theta}(t)$ when numerically integrated for the same initial conditions.

To illustrate this, the following parameters are considered for the bodies of the mechanism: $r = 0.3$ m, $L = 0.7$ m, $h = 0.15$ m, $m^{(1)} = 0.5$ kg, $m^{(2)} = 1$ kg, $g = 9.81$ m/s^2.

Figure 7 shows the free oscillation ($M(t) = 0$) of the system when subject to initial condition given by $\theta_0 = \pi/4$ rad and $\dot{\theta}_0 = 0$ rad/s. It can be seen that the results obtained by integrating Eqs. (36) and (39) coincide. Since the mechanical system is conservative, its total mechanical energy is conserved, as shown in Fig. 8.

The system response due to a forcing moment $M(t) = 5 + \sin(10\pi t)$ N·m is shown in Fig. 9. Once again, the results obtained for $\theta(t)$ and $\dot{\theta}(t)$ are the same, regardless of which version of the equation of motion is integrated.

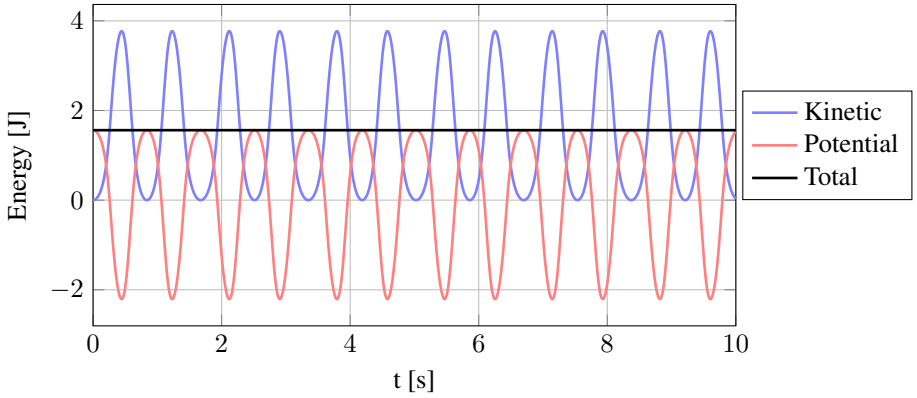

Figure 8: **Conservation of mechanical energy for the slider-crank mechanism due to initial conditions $\theta_0 = \pi/4$ rad and $\dot{\theta}_0 = 0$ rad/s.**

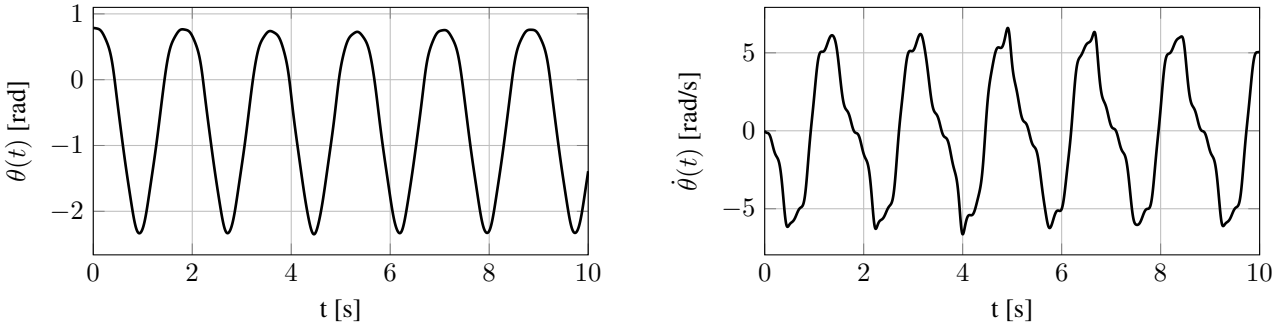

Figure 9: **$\theta(t)$ and $\dot{\theta}(t)$ for the slider-crank mechanism driven by a forcing moment $M(t)$.**

4. CONCLUSION

This paper presented how Green's Theorem can be used to promote interdisciplinarity between mathematical concepts and engineering applications. Through it, simple algebraic expressions that allow calculating the area, centroid position, moments and products of inertia of plane shapes were determined and validated against four plane shapes of increasing complexity. The expressions developed were applied in the study of the dynamics of a slider-crank mechanism. It was shown that Euler's equations lead to the same response for the mechanical system, whether written in an inertial frame of reference or in one fixed to the body. It is expected that the methodology presented can serve as a tool to promote interdisciplinarity in mathematics disciplines of vector calculus, as well as in engineering courses related to statics and dynamics of rigid bodies. As an extension of this work, it is recommended to further develop the methodology for dealing with three-dimensional bodies. One possible way is to replace Green's Theorem with the Divergence Theorem or Stokes' Theorem and make the necessary adaptations.

5. ACKNOWLEDGMENTS

M.B.R.Fernandes is grateful to the São Paulo State Research Foundation (FAPESP) for his doctorate scholarship (grant #19/19921-5). All authors also acknowledge FAPESP for supporting their work through a thematic grant (Periodic structure design and optimization for enhanced vibroacoustic performance: ENVIBRO, #18/15894-0). D.A.Rade acknowledges the Brazilian Research Council (CNPq) for grants #310633/2013-3 and #312068/2020-4.

6. APPENDIX A

The position vector of the vertices that form the crank can be readily written into the crank-fixed reference frame, $\mathscr{B}_1$:

$$ {}_{\mathscr{B}_1}\mathbf{r}_{\mathrm{P}_1/\mathrm{O}} = [0 \quad -h/2 \quad 0]^\top, \quad {}_{\mathscr{B}_1}\mathbf{r}_{\mathrm{P}_2/\mathrm{O}} = [r \quad -h/2 \quad 0]^\top, \quad {}_{\mathscr{B}_1}\mathbf{r}_{\mathrm{P}_3/\mathrm{O}} = [r \quad h/2 \quad 0]^\top, \quad {}_{\mathscr{B}_1}\mathbf{r}_{\mathrm{P}_4/\mathrm{O}} = [0 \quad h/2 \quad 0]^\top, \tag{40} $$

where the vertices $\mathrm{P}_1, \ldots, \mathrm{P}_4$ are defined from point O (cf. Fig. 5), traversing the boundary of the crank in a counter-clockwise direction.

These vectors can be written with respect to the inertial frame using the transformation matrix $\mathbf{T}_\theta$:

$$ {}_{\mathscr{I}}\mathbf{r}_{\mathrm{P}_j/\mathrm{O}} = \mathbf{T}_\theta^\top \cdot {}_{\mathscr{B}_1}\mathbf{r}_{\mathrm{P}_j/\mathrm{O}}, \quad j = 1, \ldots, 4, \tag{41} $$

where:

$$\mathbf{T}_\theta = \begin{bmatrix} \cos\theta & \sin\theta & 0 \\ -\sin\theta & \cos\theta & 0 \\ 0 & 0 & 1 \end{bmatrix}. \tag{42}$$

The components of the previous position vectors can be fed into the expressions shown in Tab. 1 to produce the moments of inertia $J^{(1)}_{xx,\mathrm{O}}$ and $J^{(1)}_{yy,\mathrm{O}}$:

$$J^{(1)}_{xx,\mathrm{O}} = m^{(1)}\left(\frac{h^2}{12}\cos^2\theta + \frac{r^2}{3}\sin^2\theta\right), \quad J^{(1)}_{yy,\mathrm{O}} = m^{(1)}\left(\frac{h^2}{12}\sin^2\theta + \frac{r^2}{3}\cos^2\theta\right). \tag{43}$$

From both, the moment of inertia about the z-axis can be computed as:

$$J^{(1)}_{zz,\mathrm{O}} = \iint_D \left(x^2+y^2\right)\mathrm{d}m, \quad = J^{(1)}_{xx,\mathrm{O}} + J^{(1)}_{yy,\mathrm{O}} = m^{(1)}\left(\frac{h^2}{12}+\frac{r^2}{3}\right). \tag{44}$$

Although the moments of inertia $J^{(1)}_{xx,\mathrm{O}}$ and $J^{(1)}_{yy,\mathrm{O}}$ vary with θ, and therefore with time, the moment of inertia $J^{(1)}_{zz,\mathrm{O}}$ is constant. This is because the distance from the crank's center of mass to the z-axis is constant, while the distance to the x and y axes vary as a function of θ.

7. APPENDIX B

Based on the free-body diagram for the mechanism bodies shown in Fig. 6, Newton's equations for the crank can be written as:

$${}_{\mathscr{I}}\mathbf{F}_\mathrm{O} + {}_{\mathscr{I}}\mathbf{F}_\mathrm{A} + {}_{\mathscr{I}}\mathbf{F}_{\mathrm{CM_1}} = m^{(1)} \cdot {}_{\mathscr{I}}\mathbf{a}_{\mathrm{CM_1}}, \tag{45}$$

which yields:

$$\begin{aligned} F_{\mathrm{O}x} + F_{\mathrm{A}x} &= -m^{(1)}\frac{r}{2}\left(\cos\theta\dot\theta^2 + \sin\theta\ddot\theta\right), \\ F_{\mathrm{O}y} + F_{\mathrm{A}y} - gm^{(1)} &= -m^{(1)}\frac{r}{2}\left(\sin\theta\dot\theta^2 - \cos\theta\ddot\theta\right). \end{aligned} \tag{46}$$

Euler's equations for the crank, using frame $\mathscr{B}_1$, can be written as:

$${}_{\mathscr{B}_1}\mathbf{r}_{\mathrm{A/O}} \times {}_{\mathscr{B}_1}\mathbf{F}_\mathrm{A} + {}_{\mathscr{B}_1}\mathbf{r}_{\mathrm{CM_1/O}} \times {}_{\mathscr{B}_1}\mathbf{F}_{\mathrm{CM_1}} = {}_{\mathscr{B}_1}\mathbf{J}^{(1)}_\mathrm{O} \cdot {}_{\mathscr{B}_1}\dot{\boldsymbol{\omega}}^{(1)} + {}_{\mathscr{B}_1}\boldsymbol{\omega}^{(1)} \times \left({}_{\mathscr{B}_1}\mathbf{J}^{(1)}_\mathrm{O} \cdot {}_{\mathscr{B}_1}\boldsymbol{\omega}^{(1)}\right) + m^{(1)} \cdot {}_{\mathscr{B}_1}\mathbf{r}_{\mathrm{CM/O}} \times {}_{\mathscr{B}_1}\mathbf{a}_\mathrm{O}, \tag{47}$$

which can be simplified to:

$$M(t) - r(F_{\mathrm{A}x}\sin\theta - F_{\mathrm{A}y}\cos\theta) - m^{(1)}g\frac{r}{2}\cos\theta = J^{(1)}_{zz,\mathrm{O}}\ddot\theta, \tag{48}$$

where $J^{(1)}_{zz,\mathrm{O}}$ is given by Eq. (44).

Finally, Newton's equations for the connecting rod can be written as:

$$-{}_{\mathscr{I}}\mathbf{F}_\mathrm{A} + {}_{\mathscr{I}}\mathbf{F}_\mathrm{B} + {}_{\mathscr{I}}\mathbf{F}_{\mathrm{CM_2}} = m^{(2)} \cdot {}_{\mathscr{I}}\mathbf{a}_{\mathrm{CM_2}}, \tag{49}$$

which generates:

$$\begin{aligned} F_{\mathrm{A}x} &= m^{(2)}\left(\frac{L}{2}\sin\beta\ddot\beta + r\cos\theta\dot\theta^2 + r\sin\theta\ddot\theta + \frac{L}{2}\cos\beta\dot\beta^2\right), \\ F_{\mathrm{B}y} - F_{\mathrm{A}y} - gm^{(2)} &= m^{(2)}\left(\frac{L}{2}\sin\beta\dot\beta^2 - \frac{L}{2}\cos\beta\ddot\beta - r\sin\theta\dot\theta^2 + r\cos\theta\ddot\theta\right). \end{aligned} \tag{50}$$

8. REFERENCES

Alves, M., Coutinho, C., Rocha, A.M.A.C. and Rodrigues, C., 2016. "Fatores que influenciam a aprendizagem de conceitos matemáticos em cursos de engenharia: Um estudo exploratório com estudantes da universidade do minho". *Revista Portuguesa de Educação*, Vol. 29, No. 1, p. 259. doi:10.21814/rpe.5998. URL `https://doi.org/10.21814/rpe.5998`.

Craig, T.S., 2013. "Conceptions of mathematics and student identity: implications for engineering education". *International Journal of Mathematical Education in Science and Technology*, Vol. 44, No. 7, pp. 1020–1029. doi: 10.1080/0020739x.2013.823521. URL `https://doi.org/10.1080/0020739x.2013.823521`.

Crisco, J. and McGovern, R., 1997. "Efficient calculation of mass moments of inertia for segmented homogenous three-dimensional objects". *Journal of Biomechanics*, Vol. 31, No. 1, pp. 97–101. doi:10.1016/s0021-9290(97)00108-5. URL https://doi.org/10.1016/s0021-9290(97)00108-5.

Faulkner, B., Earl, K. and Herman, G., 2019. "Mathematical maturity for engineering students". *International Journal of Research in Undergraduate Mathematics Education*, Vol. 5, No. 1, pp. 97–128. doi:10.1007/s40753-019-00083-8. URL https://doi.org/10.1007/s40753-019-00083-8.

Flegg, J., Mallet, D. and Lupton, M., 2012. "Students' perceptions of the relevance of mathematics in engineering". *International Journal of Mathematical Education in Science and Technology*, Vol. 43, No. 6, pp. 717–732. doi:10.1080/0020739x.2011.644333. URL https://doi.org/10.1080/0020739x.2011.644333.

Ha, J.L., Fung, R.F., Chen, K.Y. and Hsien, S.C., 2006. "Dynamic modeling and identification of a slider-crank mechanism". *Journal of Sound and Vibration*, Vol. 289, No. 4-5, pp. 1019–1044. doi:10.1016/j.jsv.2005.03.011. URL https://doi.org/10.1016/j.jsv.2005.03.011.

Harris, D., Black, L., Hernandez-Martinez, P., Pepin, B., Williams, J. and with the TransMaths Team, 2015. "Mathematics and its value for engineering students: what are the implications for teaching?" *International Journal of Mathematical Education in Science and Technology*, Vol. 46, No. 3, pp. 321–336. doi:10.1080/0020739x.2014.979893. URL https://doi.org/10.1080/0020739x.2014.979893.

Hibbeler, R., 2014. *Statics and Mechanics of Materials*. Pearson Prentice Hall. ISBN 9780133451603.

House, D. and Keyser, J., 2017. *Foundations of Physically Based Modeling and Animation*. CRC Press, Taylor & Francis Group. ISBN 9781482234602.

Kreyszig, E., 2010. *Advanced Engineering Mathematics*. John Wiley & Sons. ISBN 9780470458365.

Manseur, Z., Ieta, A. and Manseur, R., 2010. "Modern mathematics requirements in a developing engineering program". In *2010 Annual Conference & Exposition Proceedings*. ASEE Conferences. doi:10.18260/1-2–16997. URL https://doi.org/10.18260/1-2-16997.

Marsden, J., 2011. *Vector Calculus*. W. H. Freeman. ISBN 9781464119415.

Press, W., Teukolsky, S., Vetterling, W. and Flannery, B., 2007. *Numerical Recipes 3rd Edition: The Art of Scientific Computing*. Cambridge University Press. ISBN 9780521880688.

Rade, D., 2018. *Cinemática e Dinâmica para Engenharia*. Elsevier. ISBN 9788535281873.

Santos, I., 2001. *Dinâmica de sistemas mecânicos: modelagem, simulação, visualização, verificação*. Makron. ISBN 9788534611107.

Willcox, K. and Bounova, G., 2004. "Mathematics in engineering: Identifying, enhancing, and linking the implicit mathematics curriculum". In *2004 Annual Conference Proceedings*. ASEE Conferences. doi:10.18260/1-2–13246. URL https://doi.org/10.18260/1-2-13246.

Wood, L.N., Mather, G., Petocz, P., Reid, A., Engelbrecht, J., Harding, A., Houston, K., Smith, G.H. and Perrett, G., 2012. "UNIVERSITY STUDENTS' VIEWS OF THE ROLE OF MATHEMATICS IN THEIR FUTURE". *International Journal of Science and Mathematics Education*, Vol. 10, No. 1, pp. 99–119. doi:10.1007/s10763-011-9279-y. URL https://doi.org/10.1007/s10763-011-9279-y.

9. RESPONSIBILITY NOTICE

The authors are solely responsible for the printed material included in this paper.